Turk J Phys
30 (2006) , 277 – 285.

First Principles Approach to $BaTiO_3$

M. ULUDOĞAN, T. ÇAĞIN
Texas A&M University, Artie McFerrin Department of Chemical Engineering,
519 Jack E. Brown Engineering Building, 3122 TAMU, College Station, TX 77843-3122, USA

Received 18.07.2006

Abstract

We present state of art first-principles study on the static and dynamic properties of $BaTiO_3$, a typical ferroelectric material. Here, structure, equation of state, phase stability, and phase transformations of $BaTiO_3$ studied in Generalized Gradient Approximation. Furthermore, properties such as, Born effective charges, optical dielectric constant and phonon spectra are calculated from Density Functional Perturbation Theory.

1. Introduction

Since the discovery of ferroelectricity in Rochelle salt crystal [1] by Valasek in 1921, followed by the discovery of the ferroelectricity in ABO_3 perovskite $BaTiO_3$ [2] in 1945, new materials have successfully been designed for a variety of industrial and commercial applications such as high-dielectric constant capacitors, ferroelectric thin film memories, piezoelectric sonars, positive temperature coefficient sensors and switches.

Designing new configurations of ferroelectric materials for performance properties challenges material designers. Thin film ferroelectrics for applications ranging from tunable microwave devices to infrared (IR) detectors to achieve a tunability/loss tangent ratio of 100 at 100 GHz. Thus, the composition and nanostructure to maximize tunability (ability to change the dielectric constant with an electric field) is essential while minimizing the dielectric loss tangent. For a better theoretical description of these materials, different phases of these materials have been studied extensively.

The aim of this work is to create a liable data to obtain a basis for force fields (FF) for larger scale modeling of ferroelectric materials. Thus, understanding the basics of ferroelectricity from quantum mechanical (QM) approaches and the use of this quantum mechanical data for the generation of a polarizable FF become a critical issue. $BaTiO_3$ is the systems of interest to be characterized by QM calculations in terms of fundamental interactions and energetics. Calculations using density functional theory (DFT) have been performed to understand the experimentally available phase transitions. Thus, $BaTiO_3$ exhibits three ferroelectric phase transitions from cubic to tetragonal, from tetragonal to orthorhombic and finally from orthorhombic to rhombohedral as the temperature goes down.

In the following section, details of the calculations will be presented. Methods used, structures and optimization procedure for internal degrees of freedom for each structure will be discussed in this section. In Sec. III.A, results of the structure optimization, equation of state (EOS), will be presented. Correspondence between this work and the experiment and other theoretical works will be shown. In Sec. III.B, importance of Born effective charges on bonding, ferroelectricity and longitudinal optical- transverse optical (LO-TO) mode splitting will be addressed.

2. Methods of Calculation

Calculations of EOS have been performed in the general framework of DFT [3, 4, 5] using projector augmented wave method (PAW)[6]. Exchange-correlation used was Perdew-Burke-Ernzerhof (PBE) [7] generalized gradient approximation (GGA). Kinetic energy cutoff of the electronic wavefunctions was expanded in plane waves up to 600 eV. Integrals over the Brillouin zone were summed on a Monkhorst-Pack mesh [8] of 10×10×10. The 5s, 5p and 6s levels of Ba, the 3s, 3p, 3d and 4s of Ti, the 2s and 2p of O were treated as valence states. Vienna Ab-initio software package, VASP [9, 10] was used for the EOS and structural optimization calculations.

Most of ABO_3 type perovskites have similar stable phases at various temperatures. $BaTiO_3$ has four stable phases, namely, rhombohedral, orthorhombic, tetragonal and cubic phases at temperatures in the increasing order while $PbTiO_3$ has only two stable phases of tetragonal and cubic. All of these phases have some internal degrees of freedom (except cubic phase) that need to be optimized. Thus, DFT calculations have been performed at high precision (high kinetic energy cutoff and Monkhorst-Pack mesh) in order to obtain the ferroelectric phases precisely. No minimization was done in cubic phase. At desired volume, total energy and diagonal hydrostatic pressure tensor were obtained. Volume of the cubic cell was expanded 10% and was contracted 15% with respect to zero pressure state in order to get the EOS. EOS used in the calculations was Rose's universal binding curve [11]. In the ferroelectric phases, the optimization procedure of the structures was rather complicated since number of degrees of freedom increased for the lower symmetry structures. Tetragonal, orthorhombic and rhombohedral structures contained respectively four, six and five atomic degrees of freeedom. A conjugate-gradient algorithm [12] was used for minimization process. First of all, ions were relaxed into their instantaneous ground state by keeping the volume and cell shape fixed. Then with the relaxed positions, only the cell shape was optimized at fixed volume. This minimization process has been followed at constant volume since the forces between ions were less than 0.001 eV/Å. Same procedure were followed for the volumes up to 10% expansion and down to 15% contraction of the zero pressure state.

For cubic structure, there was no need for minimization. Tetragonal structure was optimized by letting the fractional coordinates of the ions change in the way symmetry allows (distortion in z direction) at fixed c/a ratio by keeping the volume fixed. Then, by using the optimized fractional coordinates of the ions, c/a ratio was optimized at constant volume. Thus, c/a ratio, Δ_{T-Ti}, Δ_{T-O_1} and Δ_{T-O_2} were the quantities that were optimized during the minimization. In orthorhombic phase, lattice parameters a, b, c and Δ_{O-Ti}, Δ_{O-O_1}, Δ_{O-O_2} and Δ_{O-O_3} were the degrees of freedom. Lattice parameter a ($a = b = c$), the angle α ($\alpha = \beta = \gamma$), Δ_{R-Ti}, Δ_{R-O_1} and Δ_{R-O_2} were the optimized quantities for rhombohedral phase. Similar optimization scheme with tetragoal phase was used in orthorhombic and rhombohedral phases. Atomic positions are shown in Table 1.

ABINIT *ab initio* software package [15, 16] was used in order to obtain response function calculations within the recent advances in density functional theory. Within ABINIT, PBE exchange-correlation formalism with a norm-conserving pseudopotential approach [17, 18] was used with the same valence states defined above. Electronic wave functions were expanded in plane waves up to 1360 eV. 4×4×4 Monkhorst-Pack mesh was accurate enough to sample the Brillouin Zone.

Dynamical matrix, Born effective charges and dielectric tensor were computed within a variational formulation [19] of the density functional perturbation theory [20]. First, calculations were carried out to determine the dynamical matrix on different meshes of q-points. Then, an interpolation was performed following the scheme proposed in Ref. [21, 22]. In this approach, long range character of the dipole-dipole contribution was subtracted from the force constant matrix in reciprocal space. Then the short range contribution to the interatomic force constants in real space is obtained from the remainder of the force constant matrix in q space using a discrete Fourier transformation [23, 24].

3. Results

3.1. Equation of State

As being the first discovered ferroelectric ceramic in early 1940s , $BaTiO_3$ has been one of the most studied cubic perovskites since then. It is paraelectric at high temperature and it has the simple cubic

Table 1. Notations of atomic positions of $BaTiO_3$ for the cubic, tetragonal, orthorhombic and rhombohedral structures in reduced coordinates. Ba atom is located at (0,0,0) position.$\Delta_{T,z}$[Ti], $\Delta_{T,z}$ [0(1)] and $\Delta_{T,z}$ [O(2)] are the distortions of Ti and O atoms in tetragonal structure, respectively [13]. In orthorhombic structure, $\Delta_{O,z}$[Ti], $\Delta_{O,z}$[O(1)], $\Delta_{O,z}$[O(2)] and $\Delta_{O,y}$[O(2)] are the distortions for Ti and O atoms [13]. Finally, in rhombohedral structure, $\Delta_{R,z}$[Ti], $\Delta_{R,z}$[O], and $\Delta_{R,x}$[O] are the distortions for Ti and O atoms, respectively [14] .

Cubic	Atom	Position
	Ba	(0,0,0)
	Ti	(0.5,0.5,0.5)
	O_1	(0.5,0.5,0.0)
	O_2	(0.5,0.0,0.5)
	O_3	(0.0,0.5,0.5)
Tetragonal	Ba	(0.0,0.0,0.0)
	Ti	(0.5,0.5,0.5+$\Delta_{T,z}$[Ti])
	O_1	(0.5,0.5,0.0+$\Delta_{T,z}$ [0(1)])
	O_2	(0.5,0.0,0.5+$\Delta_{T,z}$ [O(2)])
	O_3	(0.0,0.5,0.5+$\Delta_{T,z}$ [O(2)])
Orthorhombic	Ba	(0.0,0.0,0.0)
	Ba	(0.0,0.5,0.5)
	Ti	(0.5,0.0,0.5+$\Delta_{O,z}$ [Ti])
	Ti	(0.5,0.5,0.0+$\Delta_{O,z}$ [Ti])
	O(1)	(0.0,0.0,0.5+$\Delta_{O,z}$ [O(1)])
	O(1)	(0.0,0.5,0.0+$\Delta_{O,z}$ [O(1)])
	O(2)	(0.5,0.25+$\Delta_{O,y}$ [O(2)],0.25+$\Delta_{O,z}$ [O(2)])
	O(2)	(0.5,0.75+$\Delta_{O,y}$ [O(2)],0.75+$\Delta_{O,z}$ [O(2)])
	O(2)	(0.5,0.75-$\Delta_{O,y}$ [O(2)],0.25+$\Delta_{O,z}$ [O(2)])
	O(2)	(0.5,0.25-$\Delta_{O,y}$ [O(2)],0.75+$\Delta_{O,z}$ [O(2)])
Rhombohedral	Ba	(0.0,0.0,0.0)
	Ti	(0.5+$\Delta_{R,z}$[Ti],0.5+$\Delta_{R,z}$[Ti],0.5+$\Delta_{R,z}$[Ti])
	O_1	(0.5+$\Delta_{R,z}$[O],0.5+$\Delta_{R,z}$[O],0.0+$\Delta_{R,x}$[O])
	O_2	(0.5+$\Delta_{R,z}$[O],0.0+$\Delta_{R,x}$[O],0.5+$\Delta_{R,z}$[O])
	O_3	(0.0+$\Delta_{R,x}$[O],0.5+$\Delta_{R,z}$[O],0.5+$\Delta_{R,z}$[O])

perovskite structure. Its structure becomes tetragonal, orthorhombic and rhombohedral as the temperature goes down. At 130 °C, cubic structure (m3m point group) changes into tetragonal structure (4mm). At 5 °C, tetragonal structure transforms into orthorhombic symmetry (mm2). Finally, phase transition from orthorhombic to rhombohedral phase (3m) takes place at -90 °C. Each transition is accompanied with small atomic displacements, latent heats and macroscopic strains along the ferroelectric direction. In the ferroelectric phases, the polar axis is aligned from tetragonal phase to rhombohedral phase along $< 100 >$, $< 110 >$, $< 111 >$ directions.

There has been numerous efforts to calculate the bulk properties of barium-titanate from *ab initio* calculations. The goal of this work is to obtain accurate data from DFT for generating Polarizable Charge Equilibration (P-QEq) force field [25] parameters. This force field includes self-consistent atomic polarization and charge transfer in molecular dynamics of materials.

Energy-volume behaviors of the different crystalline phases of $BaTiO_3$ are shown in Figure 1. Energetics of the system supports that lowest symmetry structure is the structure with the lowest energy. EOS results are tabulated in Table 2. Structural parameters will be given in the Tables 3-5. Equilibrium volume and bulk modulus of the cubic structure of this work is in good agreement with experiment. As expected, local density approximation (LDA) results underestimate the equilibrium volume. Cohesive energy calculated in

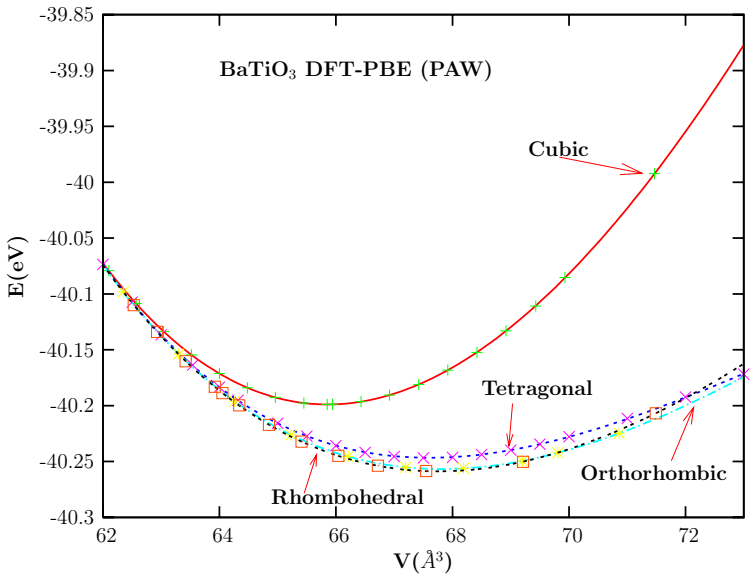

Figure 1. Energy as a function of volume for the cubic, tetragonal, orhorhombic and rhombohedral phases of $BaTiO_3$ from *ab initio* calculations using DFT-PBE. Curves stand for the EOS fitting.

this work is worse than the other theoretical calculations. In Ref. [26], authors improved the cohesive energy by expanding the system of interest volume as seven times of the equilibrium volume. But in any way, DFT calculations overestimate the binding energy of $BaTiO_3$.

In Tables 3-5, cell parameters and optimized fractional atomic coordinates for tetragonal, orthorhombic and rhombohedral structures of $BaTiO_3$ were given. Most theoretical works [14, 32, 33, 34] were performed with LDA exchange-correlation formalism. Within the local density approximation (LDA) framework, equilibrium volume of ferroelectric phases were generally underestimated. Ferroelectric instability almost vanished at optimized structures of LDA because of being sensitive to volume changes [14]. This is the reason why LDA calculations were performed at the experimental lattice constants. Also, GGA calculations overestimate the equilibrium volume of paraelectric and ferroelectric phases. In tetragonal phase of $BaTiO_3$, present work overestimated the c/a ratio as 1.051 while the experimental value was 1.011. Atomic distortions of LDA and GGA at experimental lattice constants compared well with experiment.

3.2. Born Effective Charges and Phonon Dispersion Curves

Definition of atomic charge for atoms in molecules or solids is not well defined. There are various kinds of charges in order to describe the ionicity or polarity of chemical bonds [35]: Mulliken charge, Hirshfeld charge, Bader charge, etc. All of them have their own convention. On the other hand, Born effective charge, Z^* is a fundamental quantity which shows the coupling between lattice displacements and electrostatic fields in insulators. It is also known as transverse or dynamic effective charges. It is related to the change of polarization with respect to atomic displacements [36]. Change of polarization can be experimentally measured and can give a well-defined character to Z^*.

Born effective charge is also important in terms of theoretical investigation of ferroelectric materials. Ferroelectric transitions take place from the competition of long-range Coulomb interactions and short range forces. Thus, long-range Coulomb interactions are the cause of the split between the frequencies of the longitudinal optical (LO) and transverse optical (TO) phonons [37]. The indicator to the long-range Coulomb interaction for this splitting is Born effective charge.

Axe [38] proposed experimentally an estimation of Z^* for ABO_3 compounds. He suggested anomalous effective charges. Harrison [39] also suggested from empirical studies that amplitude of Born effective charges should deviate from static ionic charges. Since the recent advances in *ab initio* techniques, Z^* has been

Table 2. EOS parameters of $BaTiO_3$ for the cubic, tetragonal, orthorhombic and rhombohedral structures: volume(lattice constant), cohesive energy, B, bulk modulus and B' , pressure derivative of bulk modulus.

	V_0(Å^3)	E_{coh} (eV)	B(GPa)	$B\prime$	Reference
Cubic	64.00	31.57	162		Exp. [13]
			135	6.4	Exp. [27]
	65.85	40.20	160.84	4.50	Present Work
	64.28	37.92	167.64	4.45	DFT-PW91 [26]
	61.30	38.23	189.00		DFT-LDA [14]
		(At expt. vol.)			
	60.93		194.2	3.68	DFT-LDA [28]
	65.45		169		DFT-GGA [29]
	65.45		175		DFT-PBE [29]
Tetragonal	67.50	40.25	82.94		Present Work
	65.95	37.96	98.60		DFT-PW91[26]
Orthorhombic	67.81	40.26	87.39		Present Work
	66.02	37.97	97.54		DFT-PW91 [26]
Rhombohedral	67.76	40.26	94.62		Present Work
	65.99	37.973	103.50		DFT-PW91 [26]

Table 3. Lattice parameters and atomic displacements in the tetragonal phase of $BaTiO_3$.

a(Å)	c(Å)	$\Delta_{T,z}$[Ti]	$\Delta_{T,z}$[O(1)]	$\Delta_{T,z}$[O(2)]	Reference
3.99095	4.0352	0.0224	-0.0244	-0.0105	[30] Exp. at 27 °C
4.00480	4.2087	0.0177	-0.0402	-0.0234	Present Work (P=0 GPa)
3.9759	4.1722	0.0188	-0.0473	-0.0266	[26] (GGA-PW91 P=0 GPa)
3.99095	4.0352	0.0142	-0.0227	-0.0142	Present Work at expt. volume
3.99095	4.0352	0.0165	-0.0272	-0.0156	[26](GGA-PW91 at expt. volume)
3.994	4.036	0.0143	-0.0307	-0.0186	[14] (LDA at expt. volume)
3.986	4.026	0.015	-0.023	-0.014	[31] Exp.
		0.014	-0.0249	-0.0156	[32]
		0.0135	-0.0250	-0.0150	[33]
4.000	4.000	0.0138	-0.0253	-0.0143	[34]

Table 4. Lattice parameters and atomic displacements of $BaTiO_3$ in the orthorhombic phase.

	Expt. [30] -43 °C	LDA [14]	[31] -10 °C	Present Work	Present Work Expt. Volume
a(Å)	3.9841	3.984	3.990	3.9914	3.9841
b(Å)	5.6741	5.674	5.669	5.7830	5.6741
c(Å)	5.6916	5.692	5.682	5.8223	5.6916
$\Delta_{O,z}$[Ti]	0.0079	0.0127	0.010	0.0159	0.0121
$\Delta_{O,z}$[O(1)]	-0.0233	-0.0230	-0.016	-0.0206	-0.0125
$\Delta_{O,z}$[O(2)]	-0.0146	-0.0162	-0.010	-0.0234	-0.0149
$\Delta_{O,y}$[O(2)]	-0.0145	-0.0146	-0.010	-0.0075	-0.0037

Table 5. Lattice parameters and atomic displacements of $BaTiO_3$ in rhombohedral phase.

a(Å)	α (deg)	$\Delta_{R,z}$[Ti]	$\Delta_{R,x}$[O]	$\Delta_{R,z}$[O]	Reference
4.003	89.84	-0.013	0.011	0.0191	[30] Exp.
4.001	89.87	-0.011	0.013	0.0192	[14]
4.000	90.00	-0.012	0.010	0.0195	[34]
4.073	89.74	-0.0150	0.0141	0.0245	Present Work
4.042	89.77	-0.0148	0.0137	0.0246	[26]

Table 6. Born effective charges and optical dielectric constant of $BaTiO_3$ in the cubic structure.

Z_{Ba}	Z_{Ti}	$O_\perp$	$O_\parallel$	ε_∞	Reference
2.9	6.7	-2.4	-4.8	5.40[a]	Exp. [38]
				5.24[b]	Exp [45]
2.71	7.80	-2.15	-6.21	7.28	Present Work
2.69	7.41	-2.14	-5.82	6.80	Present Work
					(a=4.00 Å)
2.74	7.32	-2.14	-5.78	6.75	DFT-LDA [23]
2.75	7.16	-2.11	-5.69		DFT-LDA [42]
2.77	4.83	-1.42	-4.76		MD (P-QEq) [25]
1.93	6.45	-2.3	-3.79		MD [46]
					(Dynamic shell model)

[a] ε_∞ was obtained by extrapolating to zero frequency index of refraction measurements [47].
[b] Experimental values for $\varepsilon_\infty(0)$ observed in the visible light range [45] extrapolated to the optical $w = 0$ limit using dispersion relation $\varepsilon - 1 = C/(w_0^2 - w^2)$ where C and w_0 are constants.

accessible from theoretical calculations by using perturbation theory [19] or finite difference of polarization [36]. With the results obtained from first-principles calculations [40–44] Z^* was confirmed to be anomalously large , sometimes as much as twice of the nominal ionic charge.

In Table 6, Born effective charges and optical dielectric constant for $BaTiO_3$ is presented. Calculations have been performed at optimized zero-pressure state at lattice constant of 4.052 and experimental value 4.00 Å. Ba and Ti atoms have isotropic charge tensor, while O atoms have perpendicular, $O_\perp$ and parallel, $O_\parallel$ charge tensor components to Ti-O bonding. Born effective charges of Ti and $O_\parallel$ are quite larger than their nominal values (+4 for Ti and -2 for O). Essentially, these anomalous charges reveal the mixed ionic and covalent character of the bond. When ionic bond overcomes covalent bond between O-2p and Ti-3d states, short range repulsions become strong enough to stabilize the cubic phase. Therefore, it can be concluded that hybridization between the Ti and O is essential to weaken the short range repulsions and allow the ferroelectric transition [41, 42, 48].

Optical dielectric constant (calculated at experimental lattice constant) 6.80 is 26% larger than the experimental value 5.40 (as expected within DFT). This difference in optical dielectric coefficient will affect the value of the highest longitudinal optic mode. After replacing the theoretical dielectric constant with the experimental value, frequency of the highest longitudinal optic (LO) mode changes from 82.87 to 89.32 meV. Experimental value of this highest mode is 95.73 meV. By using the experimental dielectric constant, Ph. Ghosez et al.[23] shifted their highest (LO) from 78.23 to 86.29 meV.

Phonon band structure of BaTiO3 is plotted in Figure 2 along high symmetry lines $\Gamma - X - M - \Gamma - R - M$. Negative frequency in the plot shows the imaginary frequency associated with unstable modes. However, experimentally observed frequencies have real values while theoretical calculations show unstable phonon modes which are the driving force for ferroelectric phase transitions. As discussed by Ph. Ghosez et al. [23], two transverse modes are unstable at the Γ point. Along the $\Gamma - M$ and $X - M$ lines, one of these two stabilizes. Finally, both of the unstable modes become stable in the vicinity of R-point. Frequencies at high

symmetry points are reported in Table 7.

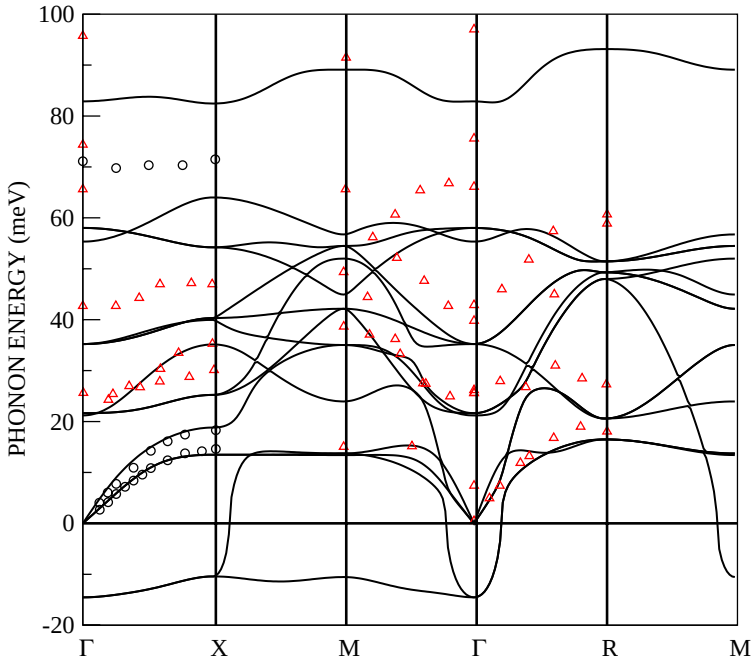

Figure 2. Phonon dispersion curves of $BaTiO_3$ at experimental lattice constant. Theoretical result shows an agreement with the experimental data: (○) [49], (△) [50].

Table 7. Computed phonon frequencies (meV) of cubic $BaTiO_3$ at experimental lattice constant of 4.0 Å, at Γ, X, M and R. Second frequency set was calculated by using DFT-LDA at experimental lattice constant by Ph. Ghosez *et al.* [23].

q-point	Label	Freq. Present Work	Label	Freq. Present Work	Label	Freq.[23]	Label	Freq.[23]
Γ	Γ_{15}(TO)	14.53 i	Γ	35.21	Γ_{15}(TO)	27.15 i	Γ	34.84
	Γ_{15}(A)	0	Γ_{15}(LO)	55.34	Γ_{15}(A)	0	Γ_{15}(LO)	55.17
	Γ_{15}(LO)	21.20	Γ_{15}(TO)	58.02	Γ_{15}(LO)	19.71	Γ_{15}(TO)	56.16
	Γ_{15}(TO)	21.63	Γ_{15}(LO)	82.87	Γ_{15}(TO)	20.58	Γ_{15}(LO)	78.23
X	X_5	10.43 i	X_3	39.95	X_5	23.43 i	X_3	39.92
	$X_{5'}$	13.48	$X_{5'}$	40.32	$X_{5'}$	12.89	$X_{5'}$	40.91
	$X_{2'}$	18.82	X_5	54.21	$X_{2'}$	18.10	X_5	52.20
	X_5	25.22	X_1	64.00	X_5	24.05	X_1	64.10
	X_1	35.14	$X_{2'}$	82.44	X_1	32.24	$X_{2'}$	77.74
M	$M_{3'}$	10.54 i	M_5	44.94	$M_{3'}$	20.71 i	M_5	42.65
	$M_{2'}$	13.42	M_2	51.99	$M_{2'}$	12.77	M_2	43.89
	$M_{5'}$	13.73	$M_{5'}$	54.48	$M_{5'}$	12.89	$M_{5'}$	53.93
	M_3	23.95	M_1	56.74	M_3	25.79	M_1	56.54
	$M_{5'}$	35.03	M_4	89.09	$M_{5'}$	33.48	M_4	84.68
	$M_{3'}$	42.15			$M_{3'}$	41.29		
R	R_{15}	16.48	$R_{25'}$	49.30	R_{15}	15.87	$R_{25'}$	47.86
	R_{25}	20.59	R_{15}	51.45	R_{25}	22.57	R_{15}	51.33
	$R_{12'}$	47.99	$R_{2'}$	93.14	$R_{12'}$	38.93	$R_{2'}$	88.90

4. Conclusion

In this study, structure and equation of state of stable phases of $BaTiO_3$ were investigated by means of DFT. Computed results were compared with the available experimental data and theoretical calculations. Effect of Born effective charges to the stability of ferroelectricity and their impact on Ti-O bond were discussed. Besides, the importance of LO-TO mode splitting was addressed in terms of dynamical charges and optical dielectric constant. Finally, phonon dispersion relation of BaTiO3 were calculated. Soft modes obtained in this work was at least consistent with the other DFT calculation and available experimental results. The highest longitudinal optical mode was closer to experiment result than other theoretical work [23].

References

[1] J. Valasek, *Phys. Rev.*, **17**, (1921), 475-81.

[2] R. W. Gray, U.S. Pat. No. 2 486 560, 1949.

[3] P. Hohenberg and W. Kohn, *Phys. Rev.*, **136**, (1964), 864A.

[4] W. Kohn and L. J. Sham, *Phys. Rev.*, **140**, (1965), 1133B.

[5] M. C. Payne, M. P. Teter, D. C. Allan, T. A. Arias and J. D. Joannopoulos, *Rev. Mod. Phys.*, **64**, (1992), 1045.

[6] G. Kresse, and J. Joubert, *Phys. Rev. B*, **59**, (1999), 1758.

[7] J. P. Perdew, K. Burke, and M. Ernzerhof, *Phys. Rev. Lett.*, **77**, (1996), 3865.

[8] H. J. Monkhorst and J. D. Pack, *Phys. Rev. B*, **13**, (1977), 5188.

[9] G. Kresse and J. Hafner, *Phys. Rev. B*, **47**, (1993), RC558.

[10] G. Kresse and J. Furthmüller, *Phys. Rev. B*, **54**, (1996), 11169.

[11] J. H. Rose, J. R. Smith, F. Guinea and J. Ferrante, *Phys. Rev. B*, **29**, (1984), 2963.

[12] W. H. Press, B.P. Flannery, S.A. Teukolsky and W.T. Vetterling, *Numerical Recipes*, (Cambridge University Press, New York, 1986).

[13] K. H. Hellwege, A. M. Hellwege (Eds.), *Ferroelectrics and Related Substances*, New Series Vol. 3, Landolt-Bornstein, (Springer, Berlin, 1969) (group III).

[14] P. Ghosez, X. Gonze and J.-P. Michenaud, *Ferroelectrics*, **220**, (1999), 1.

[15] X. Gonze, J.-M. Beuken, R. Caracas, F. Detraux, M. Fuchs, G.-M. Rignanese, L. Sindic, M. Verstraete, G. Zerah, F. Jollet, M. Torrent, A. Roy, M. Mikami, Ph. Ghosez, J.-Y. Raty, D. C. Allan, *Computational Materials Science*, **25**, (2002), 478-492.

[16] X. Gonze, G.-M. Rignanese, M. Verstraete, J.-M. Beuken, Y. Pouillon, R. Caracas, F. Jollet, M. Torrent, G. Zerah, M. Mikami, Ph. Ghosez, M. Veithen, J.-Y. Raty, V. Olevano, F. Bruneval, L. Reining, R. Godby, G. Onida, D. R. Hamann, and D. C. Allan. *Zeit. Kristallogr.*, **220**, (2005), 558-562.

[17] I. Grinberg, N. J. Ramer, and A. M. Rappe, *Phys. Rev. B*, **62**, (2000), 2311.

[18] A. M. Rappe, K. M. Rabe, E. Kaxiras and J. D. Joannopoulos, *Phys. Rev. B*, **41**, (1990), 1227.

[19] X. Gonze, D. C. Allan and M. P. Teter, *Phys. Rev. Lett.*, **68**, (1992), 3603; C. Lee, Ph Ghosez and X. Gonze, *Phys. Rev. B*, **50**, (1994), 13379.

[20] N. E. Zein, *Sov. Phys., Solid State*, **26**, 1825 (1984): S. Baroni, P. Giannozzi and A. Testa, *Phys. Rev. Lett.*, **58**, (1987), 1861.

[21] P. Giannozzi, S. de Gironcoli, P. Pavone and S. Baroni, *Phys. Rev. B*, **43**, (1991), 7231.

[22] X. Gonze, J.-C Charlier, D. C. Allen and M. P. Teter, *Phys. Rev. B*, **50**, (1994), 13035.

[23] Ph. Ghosez, X. Gonze and J.-P. Michenaud, *Ferroelectrics*, **206-207**, (1998), 205.

[24] Ph. Ghosez, E. Cockayne, U. V. Waghmare and K. M. Rabe, *Phys. Rev. B*, **60**, (1999), 836.

[25] Q. Zhang, "Atomistic Simulations of $BaTiO_3$", Ph. D. Thesis, California Institute of Technology, Pasadena California (2004).

[26] M. Uludoğan, T. Çağın and W.A. Goddard III, *Mater. Res. Soc. Symp. Proc.*, **718**, (2002), 341.

[27] Ph. Pruzan, D. Gourdain, J. C. Chrvin, B. Canny, B. Couzinet and M. Hanfland, *Solid State Comm.*, **123**, (2002), 21.

[28] R. Khenata, M. Sahnoun, H. Baltache, M. Rerat, A. H. Rashek, N. Illes and B. Bouhafs, *Solid State Comm.*, **136**, (2005), 120.

[29] S. Piskunov, E. Heifets, R. I. Eglitis and G. Borstel, *Comp. Mater. Sci.*, **29**, (2004), 165.

[30] G. H. Kwei, A. C. Lawson, S. J. L. Billinge and S.W. Cheong, *J. Phys. Chem.*, **97**, (1993), 2368.

[31] G. Shirane, H. Danner and P. Pepinsky, *Phys. Rev.*, **105**, (1957), 856.

[32] B. C. Frazer, *J. Phys. Soc. Japan*, **SB-II**, (1962), 376.

[33] J. Harada, T. Pedersen and Z. Barnea, *Acta Cryst.*, **A26**, (1970), 336.

[34] R. D. King-Smith and D. Vanderbilt, *Ferroelectrics*, **136**, (1992), 85.

[35] J. Meister and W. H. E. Schwarz, *J. Phys. Chem.*, **98**, (1994), 8245.

[36] R.D. King-Smith and D. Vanderbilt, *Phys. Rev. B*, **47**, (1993), 1651.

[37] R. H. Lyddane, R. G. Sachs and E. Teller, *Phys. Rev.*, **59**, (1941), 673.

[38] J.D. Axe, *Phys. Rev.*, **157**, (1967), 429.

[39] W. A. Harrison, *Electronic Structure and the Properties of Solids*, (Freeman, San Fransisco, 1980).

[40] Ph. Ghosez, X. Gonze, Ph. Lambin and J.-P. Michenaud, *Phys. Rev. B*, **51**, (1995), 6765.

[41] P. Ghosez, J.-P. Michenaud and X. Gonze, *Phys. Rev. B*, **58**, (1998), 6224.

[42] W. Zhong, R. D. King-Smith and D. Vanderbilt, *Phys. Rev. Lett.*, **72**, (1994), 3618.

[43] Ph. Ghosez, X. Gonze, *J. Phys.: Condens. Matter*, **12**, (2000), 9179.

[44] M. Veithen, X. Gonze and Ph. Ghosez, *Phys. Rev. B*, **66**, (2002), 235113.

[45] T. Mitsumi *et al.* (Eds.), *Oxides*, Landolt-Bornstein Numerical Data and Functional Relationships in Science and Technology, Group III, Vol. 16, Pt. a (Springer-Verlag, Berlin, 1981).

[46] S. Tinte, M. G. Stachiotti, M. Sepliarsky, R. L. Migoni and C. O. Rodriguez, *J. Phys.: Condens. Matter*, **11**, (1999), 9679.

[47] G. Burns and F. H. Dacol, *Solid State Comm.*, **42**, (1982), 9.

[48] R. E. Cohen, *Nature*, **358**, (1992), 136.

[49] G. Shirane, B. C. Frazer, V. J. Minkiewicz and J. A. Leake, *Phys. Rev. Lett.*, **19**, (1967), 234.

[50] B. Jannot, C. Escribe-Filippini and J. Bouillot, *J. Phys. C: Solid State Phys.*, **17**, (1984), 1329.